Solar RRL
www.solar-rrl.com

Design of a Color Neutral Nonpatterned Photovoltaic Window Based on Luminescent Solar Concentrator

Paolo Bernardoni, Giulio Mangherini, Alfredo Andreoli, Valentina Diolaiti, Rosamaria Marrazzo, Fabio Melchiorre, Stefano Zanardi, and Donato Vincenzi*

The necessity to fulfil buildings energy demand with different energy sources leads to an increasing integration between building components and renewable energy sources. The development of new building-integrated photovoltaics technologies requiring less silicon solar cells for active area is particularly interesting especially from a circular economy perspective. This research describes the design of five neutral color photovoltaic windows based on large area (0.61 m^2) luminescent solar concentrators co-developed by the University of Ferrara and Eni S.p.A. The windows are installed at the Eni "Renewable, New Energies and Material Science Research Centre" in Novara (Italy). The prototypes show a visible transmittance of 38.5%, exceeding that of commercially available semi-transparent photovoltaic technologies. Moreover, the evaluation of the window colorimetric properties highlights a color rendering index equal to 93.0, thus ensuring an excellent illumination quality of the building indoor. The panel electrical performance is measured indoor, at the end of the assembly process, and onsite, showing a power production ranging from 1.2 to 2.8 W and an efficiency between 0.23% and 0.48% depending on the illumination condition and the background reflectivity. Although the generated power is limited, it is already sufficient to power stand-alone small appliances and smart systems.

1. Introduction

Presently, building sector accounts for more than 30% of the global consumptions and almost 40% of the total energy-related CO_2 emissions.[1] International roadmaps aim to convert energivorous structures to zero-energy or net-zero energy buildings by supporting a wider deployment of renewable energy sources.[2,3] If efficiently harvested and stored,[4–6] solar energy represents the most promising renewable energy source to satisfy building energy demands;[7,8] however, despite the increasing penetration of PV solutions, serving purposes ranging from water decontamination to electricity production,[9–11] building-integrated photovoltaics (BIPV) have remained a relatively niche market.[12]

P. Bernardoni
G&W Altea S.r.l.
via dei Trasvolatori Atlantici, 30/A, 44124, Ferrara (FE), Italy

G. Mangherini, A. Andreoli, V. Diolaiti, D. Vincenzi
Department of Physics and Earth Sciences
University of Ferrara
via Saragat 1, 44122 Ferrara, Italy
E-mail: giulio.mangherini@unife.it

R. Marrazzo, F. Melchiorre, S. Zanardi
Renewable, New Energies and Material Science Research Center
Eni
via Fauser 4, 28100 Novara, Italy

The ORCID identification number(s) for the author(s) of this article can be found under https://doi.org/10.1002/solr.202400195.

DOI: 10.1002/solr.202400195

Since BIPV solutions directly replace building elements they must provide insulation value and structural integrity, while still functioning as PV devices that harvests energy efficiently.[13] The work of Bonomo et al.[12] underlines that due to their architectural flexibility (higher esthetic appearance and the lower cost per square meter), 44% of BIPV products installed on building facades are thin-film solutions, despite they are less energy efficient if compared to crystalline systems.

The work of Aritra Ghosh[14] underlines the growing preference in modern building architecture for the incorporation of glazed facades, particularly in commercial structures. Windows and semi-transparent façades serve as pivotal elements for the building interior health and well-being; therefore, novel BIPV technologies presenting a superior architectural flexibility with respect to thin-film panels may represent an important asset to preserve the connection between building exterior and interior.

While several innovative approaches to increase the efficiency and the architectonical integration of BIPV technologies,[15,16] thanks to their unique properties semi-transparent solutions based on luminescent solar concentrators (LSCs) are of increasing interest in academia and industry. LSC panels are able to absorb and redistribute a portion of the solar radiation impinging on them, thus reducing the number of cells for active area and harvesting both direct and diffuse solar radiation almost with the same efficiency. They are therefore much more tolerant to shading and hot spots with respect to standard PV devices.[17]

A typical LSC is composed by a slab made of a transparent material, like polymethyl methacrylate (PMMA), polycarbonate (PC), or glass, functionalized with active particles called fluorophores, which according to their nature can be classified in three main categories: aromatic compounds,[18] organometallic complexes,[19] and quantum dots.[20] When the slab is exposed to solar radiation, the fluorophores absorb part of the light striking the slab re-emitting it at a longer wavelength (fluorescence phenomenon). Since the re-emission is isotropic and the transparent material has a refractive index higher than air, a significant amount of fluorescent light is trapped inside the slab and diverted to the slab edges thanks to total internal reflection. The light reaching the slab edges can be converted into electricity by optically coupling solar cells with the pane sides. The possibility to mount solar cells along the waveguide perimeter results in the absence of busbars, collection grids, or electrodes within the light harvesting area, thus realizing PV devices having nonpatterned continuous transparent surfaces and high levels of transparency.[21,22]

The light that does not undergo total internal reflection exits the slab through the so-called escape-cone losses. Both the amount of light entrapped in the LSC and the escape-cone losses depend on the slab material.[23] The light trapped in the waveguide may either be directly diverted to the slab edges or be subjected to self-absorption.[24] The criticalities of self-absorption are related to the increment of absorption-emission processes, as the nonideal quantum yield and the emission angle of the fluorophore particles decrease the amount of trapped light reaching the slab edges. The working principle of an LSC panel is schematized in **Figure 1**.

The LSC panel optical properties can be tailored by varying the type or the concentration of the employed fluorophores.[25–27] Due to the present interest in optically neutral LSCs, several research works focused on the developing of highly transparent LSCs based on nanocrystal-assisted technology.[28–31] Similarly, the performance of slabs functionalized with quantum dots,[32–34] nanoclusters,[35] or rare-earth ion complexes[36,37] was widely investigated. These works aimed to increase the LSC panel's power conversion efficiency (PCE) by using three main approaches. The first one, embraced by Bergren et al.[21] the improvement of luminophore consisted in quantum yield, the second strategy, adopted by Li et al.[34] involved a modulation of the luminophore absorption and emission spectra, so as to decrease the reabsorption losses. The last approach followed by Rondão et al.[38] was focused on the enhancement of light absorption by matching the absorption spectrum of the luminophores with the peak of the solar spectrum.

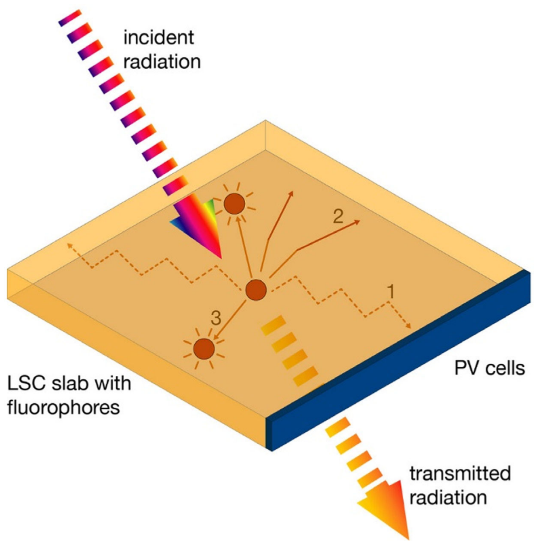

Figure 1. Operating principle of an LSC panel. In the graphical representation the functionalized slab is depicted in orange, whereas the PV cells in blue. When the light is absorbed by the fluorophores three phenomena can occur: 1) the fluorescence radiation is trapped inside the slab and guided to the solar cells, 2) the fluorescence radiation is lost outside the slab through the escape-cone, and 3) the fluorescence radiation is self-absorbed by another dye active center.

Nevertheless, all these approaches are subjected to feasibility drawbacks that severely limit the industrial scalability of LSC-based PV devices. In fact, their implementation highly increases the panel cost, thus resulting in an uncompetitive price-to-watt ratio if compared to commercial PV or BIPV technologies. State-of-the art examples are Li et al. and Lin et al. works,[39,40] which present LSCs functionalized with quantum dots (QDs). The proposed waveguides show considerable transmittance in the visible range, and a higher PCE than that of most LSCs having the same optical and geometrical characteristics. As for other very promising devices,[41] their main limitation lies in the sample dimensions (slabs with 2–25 cm sides) that are not yet compatible with the building sector.[17]

LSC panels having dimensions suitable for building integration are usually colored panels functionalized with organic dyes,[42] often designed for greenhouses,[43] or outdoor applications.[44–46] A first step in the realization of an optically balanced large-area LSC panel based on organic dyes was made by Eni that has patented a device composed by three active slabs having complementary colors, so to realize LSCs of neutral coloration.[47]

The aim of this work is to investigate a different approach for the realization of large-area color neutral devices. A simplification of the device structure has allowed the realization of large area (0.61 m^2) semi-transparent PV panels which was based on a single active slab, functionalized with a blend of fluorescent organic dyes, and whose transmitted light is further balanced through the addition of a thin film, working as an external filter. To access if the proposed configuration leads to a LSC panels having electrical characteristics compatible with the ones presented in literature, five prototypes were realized and their electrical efficiency was assessed for both indoor and outdoor characterizations. Moreover, the LSC optical properties have been evaluated by estimating their average visible transparency (AVT) and color rendering index (CRI).

2. Experimental Section

2.1. Prototype Assembly

The prototypes described in this work were designed to be installed in a preexisting façade of a test building at the Eni "Renewable, New Energies and Material Science Research Centre" in Novara (Italy) presenting window openings with an area of 0.935×0.725 m^2. Five prototypes were realized by coupling an LSC panel with a glass slab of 0.905 m $\times$ 0.695 m in a double-glazed structure that was encased in a proper framework. To be compatible with the prior window frameworks and to provide the necessary thermal insulation, the structure was made of aluminum with a PVC thermal break. The LSC slabs were manufactured by Arkema, a partner of Eni for LSC development, by using 6 mm of impact-resistant PMMA functionalized with a mix of Lumogen F Red 305 (LR305), 11 ppm, and the Eni Yellow dye 5,6-diphenoxy-4,7-bis[5-(2,6-dimethylphenyl)-2-thienyl]benzo[c]1,2,5-thia-diazole (MPDTBOP), 17.5 ppm.[48] This blend conferred to the slab a distinctive orange color as well a wide absorption range in the visible spectrum combined with a high transparency.

The photovoltaic conversion was performed by six arrays of monocrystalline passivated emitter rear contact (PERC) silicon solar cells (SunPower C50).[49] Each array consisted in a printed circuit board (PCB) that hosted 10 solar cells connected in series with a size of 24 mm × 8 mm each obtained through the mechanical dicing of a 125 mm × 125 mm SunPower C50 solar cell. Three arrays were placed on each long side of the slabs, while the remaining perimeter was covered with a high reflectivity dielectric mirror film, developed by 3M[50] and presenting an overall thickness of 104 μm and a specular reflectivity higher than 90% within the 400–775 nm range. This film application had the double purpose of reflecting most of the fluorescence light to the cell arrays[17] while protecting the surface of the LSC during the sealing procedure, as the sealant would otherwise absorbed or entrapped part of the fluorescence light.

The optical coupling between the LSC slab and the solar cells is critical for the performance of LSC devices, but other parameters should be taken into account when it comes to the choice of the glue. In particular, when exposed to temperature cycles, the difference in the coefficients of thermal expansion between PMMA ($7.0 \times 10^{-5}\ K^{-1}$) and the solar cells ($0.5 \times 10^{-5}\ K^{-1}$) or the fiberglass in the PCB ($1.3 \times 10^{-5}\ K^{-1}$ along the circuit plane) generates a thermal stress at the LSC-cells interface that must be sustained by the glue and the cells themselves. Hence, the choice of the material to join the cells on the LSC fell on Soudal Silirub PV albeit it sacrifices the maximum optical transparency, as it is a neutral monocomponent silicone developed for PV panels sealing which ensures high elasticity and no corrosion. The prototype thermal transmittance was reduced thanks to a double-layer structure, in which the LSC device and a glass slab with a thickness of 3 mm were the outer and the inner pane, respectively. On the inner glazing, a blue filter was applied (SOLAR SCREEN Spectra 40 C) that was specifically chosen to optically compensate the spectrum transmitted by the LSC slab. The double-glazing structure was then encased in an aluminum and PVC frame with a size of 0.935 m × 0.725 m which was waterproofed by mean of a low-viscosity and low corrosion silicone sealant (CHT AS1620). The electrical connections take place through two silicone-insulated wires coming out of the aluminum frame. **Figure 2** presents two renders summarizing both the window structure and its electrical connections.

2.2. Optical Characterization

The optical characterizations were performed in a dark room using an EG&G GS0895 tungsten-halogen light bulb operated at a power of 680 W, which was chosen as light source since it ensures a continuous emission in the UV-VIS-NIR sampling range. The transmitted light was collected by a quartz optic fiber and measured by using an Ocean Optics USB4000-XR1-ES Spectrometer integrating a diffraction grating and a linear CCD sensor, which can measure all the spectral components in the range 195 to 1055 nm with a sensor resolution of 0.27 nm and an optical resolution of 2 nm. A Newport *M*-ID-1.0 Iris Diaphragm was adjusted on the lamp housing's output port to achieve a beam with ≈a 20 mm diameter at a distance of 50 cm.

The dyes employed in the LSC panel were at first characterized individually at the concentrations used in the neutral window by measuring both absorption and transmission spectra of two 6 mm PMMA slabs, one functionalized with 11 ppm of LR305 and one with 17.5 ppm MPDTBOP. The samples were positioned along the optical path between the source and the integrating sphere with the exiting surface in contact with the integrating sphere's entering port, so as to collect also the LSC fluorescent light.

A background signal was obtained by acquiring a measurement in the absence of tungsten-halogen light source, Φ_{DARK}, which was then subtracted to all the acquired spectra. The transmission spectra, T, were obtained by dividing the spectral components of the spectrum acquired with the samples, $\Phi_{TSAMPLE}$, by the ones of the light source, Φ_{SOURCE}. The sum

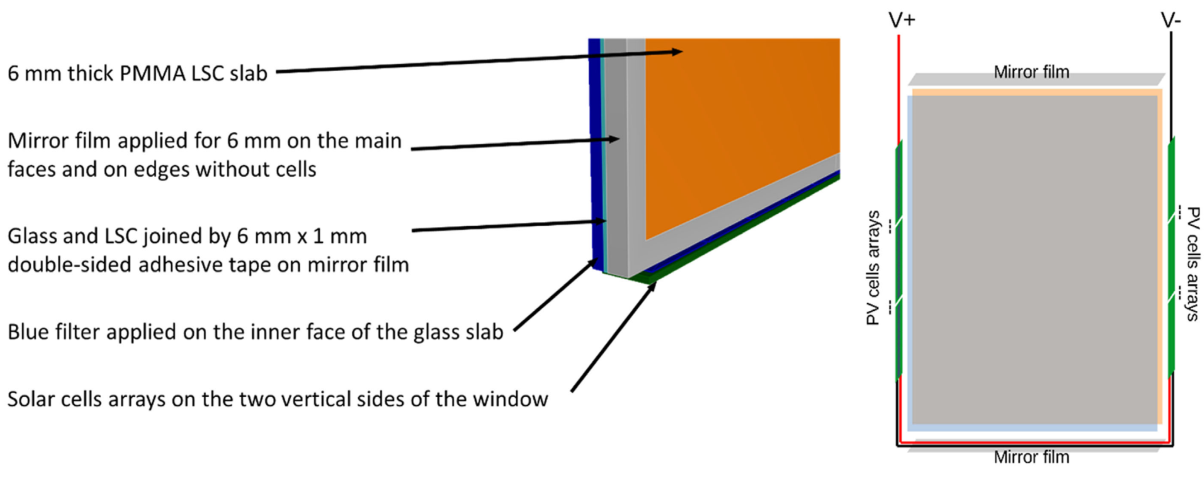

Figure 2. Render presenting on the left the main components of the PV window, and on the right its electrical connections.

of specular and diffuse reflectance, R, was computed as one minus the ratio between the signal intensity with and without a blank sample, Φ_{BLANK}, which corresponded to a 1 mm not functionalized PMMA slab or a 3 mm clear glass pane.

The former was used to evaluate the component reflected at the interface PMMA-air, thus decoupling the not transmitted portion of the spectra from the reflected one. The slab thickness was chosen to ensure a negligible absorptance of the PMMA slab in the VIS-NIR range. The latter was employed to isolate the spectral components filtered by the blue film with respect to the ones absorbed and reflected from the glass layer. The dyes and blue filter absorption spectra were calculated as 1 minus the sum of T and R. Equation (1) to 3 presents the mathematical equations adopted for the optical characterizations.

$$T = \frac{\Phi_{TSAMPLE} - \Phi_{DARK}}{\Phi_{SOURCE} - \Phi_{DARK}} \tag{1}$$

$$R = 1 - \frac{\Phi_{BLANK}}{\Phi_{SOURCE}} \tag{2}$$

$$A = 1 - R - T \tag{3}$$

Equation (1) was also used to evaluate the transmission spectra of a slab functionalized with both the dyes and the spectra of the whole window.

2.3. Colorimetric Analysis

Colorimetric analysis has been performed evaluating the window as a light source lit by sunlight whose emission spectrum is represented by solar spectrum filtered using the transmittance values. Given that the solar spectrum at the earth surface depends on time and weather conditions, for the computation of both CRI and AVT, the CIE Standard Illuminant D65 has been used as reference. D65 is also called daylight illuminant and corresponds roughly to the average midday sun spectrum in Europe and takes into account both direct and diffused components. The CRI is a parameter given by the arithmetic mean of 8 standard samples (TCS01-TCS08) that is used in colorimetry to quantitatively measure of how faithfully a light source can render the colors of different objects with respect to a reference light source. Its value was computed through a Python script and using the Color-Science (v. 0.3.16) library, an open-source Python package providing a comprehensive number of algorithms and datasets for color science, which is freely available under a New BSD License.[51] Furthermore, the value of six supplementary samples (TCS09-TCS14), not used in the CRI calculation but however useful to better understand the quality of an artificial light source, has been evaluated. Particularly interesting are the values of TCS09 (strong red) and TCS12 (strong blue), since they represent challenging values for artificial illumination devices; therefore, the analysis of these parameters for the presented device represents a further indication its colorimetric balance. Indeed, considering that the LSC panels here presented are proposed for window integration a high value in the TCS samples corresponds to a more faithful transmission of the solar spectrum, thus to a higher indoor comfort. The formula used for the CRI evaluation is reported in Equation (4)[52]

$$CRI = \frac{1}{8}\sum_{i=1}^{8}\left(100 - 4.6\sqrt{(\Delta L_i')^2 + (\Delta u_i')^2 + (\Delta v_i')^2}\right) \tag{4}$$

where $\Delta L'_i$, $\Delta u'_i$, and $\Delta v'_i$ are the difference in lightness (L') and chromaticity coordinates (u', v') between each color sample i illuminated with the spectrum emerging from the tested light source and the reference spectrum. Illuminates having a CRI value higher than 90 are considered as ideal.[53–55]

The transparency of the LSC device was evaluated by using the AVT, thus considering not only the slab transmittance spectrum but also the photopic response of human eyes to the solar photon flux. The overall AVT had been expressed according to[56]

$$AVT = \frac{\int_{\lambda_{min}}^{\lambda_{max}} T(\lambda) S(\lambda)[\frac{W}{m^2}] P(\lambda)[\frac{W}{m^2}] d\lambda}{\int_{\lambda_{min}}^{\lambda_{max}} P(\lambda)[\frac{W}{m^2}] S(\lambda)[\frac{W}{m^2}] d\lambda} \tag{5}$$

where $T(\lambda)$ is the slab transmission spectrum, $S(\lambda)$ is the solar photon flux, and $P(\lambda)$ is the photopic response of the human eye. The integration was performed over the wavelength range between 400 nm (λ_{min}) and 700 nm (λ_{max}) as it ensured to completely encompass all the visible wavelengths range within $P(\lambda)$. Although the human eye can perceive intense light at the boundaries of the 390–780 nm range, the ranges excluded from the integration does not significantly contribute to our overall perception of color.[57]

2.4. Electrical Characterization

The experimental setup for the IV and PV curves acquisition was represented by a high precision Keithley 2400 SourceMeter SMU unit controlled via a custom software developed in LabVIEW. The software was designed to automatically acquire the IV and PV curves and to calculate all the relevant parameters, namely the short circuit current (I_{SC}), the open circuit voltage (V_{OC}), the fill factor (FF), and the maximum power point (MPP), as well as its voltage (V_{MPP}) and current (I_{MPP}). Equation (6) reports the mathematical formula used to compute the PCE of the prototypes[58]

$$PCE = \frac{I_{MPP}[A] V_{MPP}[V]}{E[\frac{W}{m^2}] A[m^2]} \tag{6}$$

where I_{MPP} and V_{MPP} are, respectively, the current and voltage at maximum power point. The term A, also known as aperture area, is the device active area that for the device here presented corresponds to the slab front surface area (0.61 m^2). E is the global irradiance incident on the LSC aperture area, namely the irradiance measured by a Delta Ohm LP PYRA 02 pyranometer installed on a plane parallel to the LSC main surfaces. The prototype electrical performance was evaluated under an irradiance equal to 990 or 880 W m^{-2} depending on the test conditions.

Moreover, one window prototype was subjected to an indoor electrical performance evaluation thanks to a steady state large-area solar simulator (LASS), commercialized by Eternalsun Spire. The LASS consists of 144 lamps, of which 72 gas bulbs and 72 halogens, and it is classified as AAA+ as the light emission reaches high standards in terms of stability and homogeneity of irradiation in a 2.1×1.3 m^2 area (in accordance with the IEC 60 904-9 ed. 3). The simulator is equipped with thermocouples, to monitor the temperature reached by the device under analysis, and with a reference silicon cell (n-type B-broadband) for the irradiance measurement. The characterizations involved the electrical performance evaluation at different levels of irradiance, in particular 1000, 800, 600, 400, and 200 W m^{-2}, to simulate different levels of solar lighting. A black background was used for the indoor characterization. The IV curves were acquired by the Software ES Suite 2 developed by Eternalsun that also calculates the parameters reported above (I_{SC}, V_{OC}, FF, MPP, V_{MPP}, and I_{MPP}).

3. Results and Discussion

3.1. Optical Characterization

In **Figure 3**, the absorbance and transmittance spectra of the slabs functionalized with the two luminophores, as well as the one of the blue filter, are shown.

The spectra reported on Figure 3A, computed by using Equation (3), show that as expected the yellow dye absorbs mainly in the blue region, with an absorption peak at 430–450 nm, while the primary absorption peak of the red dye lies at 570–580 nm, thus ensuring the absorption of the yellow and orange components of the source spectrum. Moreover, the comparison of the peak heights, distribution, and full width at half maximum testifies that the blend of LR305 and MPDTBOP in a concentration ratio 1:1.6 (LR305:MPDTBOP) allowed a balanced absorption of the blue, yellow, and orange components. The blue filter was then introduced to extend the chromatic balance of the transmitted spectrum also in the red region.

As predicted, the blue thin film shows a high absorption of red and orange (see Figure 3A), but its transmittance value in the blue-green range (400–525 nm) between 70% and 85% testifies that despite of its blue color the absorbance within that spectrum region is not as low as expected. Nevertheless, it limits only the transmission of light in the deep blue and deep red regions, and the high transmittance in the 400–460 nm range ensures a warm white color as explained in Section 3.2. Colorimetric analysis.

The transmission spectra obtained thanks to Equation (1) and displayed Figure 3B also highlights as the presence of the yellow dye ensures a higher absorption of the visible spectrum at shorter wavelengths, which would not have been possible using only the red dye and the blue thin film.

The contribution of the blue filter can be further appreciated thanks to the results presented in **Figure 4**A, which displays the window transmission spectrum with and without the blue layer proving how its application increases the chromatic balance of the transmitted light. Figure 4B presents the comparison between the spectral power density of the solar radiation at AM1.5G and the spectrum filtered by the Neutral LSC, highlighting the filtration effects of the whole window in the visible range (400–700 nm).

The measurement of the prototype transmission spectrum also allows the AVT estimation that according to Equation (5) is equal to 38.5%; value which is at least 28% higher with respect to the transmittance of the majority of commercial semi-transparent PV technologies. A picture of the prototypes installed in the test building is presented in **Figure 5**. The picture presents the prototype both viewed from the LSC side installed outwards, Figure 5A, and from the glass side installed inward, Figure 5B. The inward view testifies how also from a qualitative observation the combination between the dye blend and the blue filter optically balances the light that enters the building, which shows only a slight warm tone when compared to natural sunlight.

The choice to use only one functionalized slab reduces both the assembling process and the optical losses due to multiple optical interfaces with respect to the solution having three active slabs.[47] However, the partial overlap between LR305

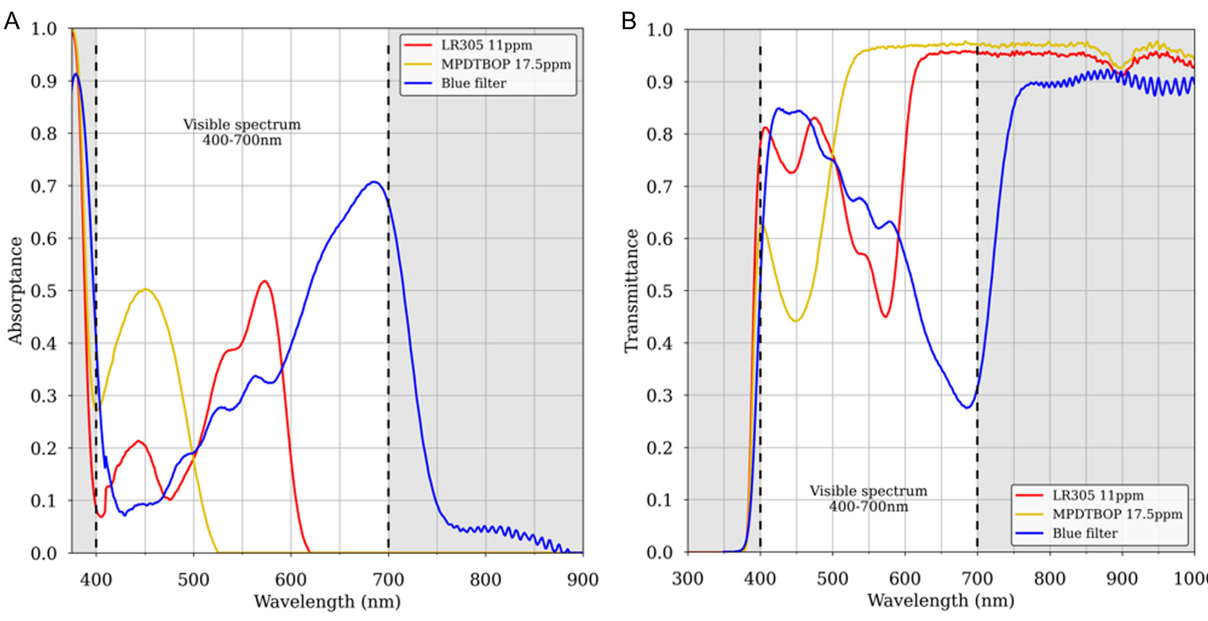

Figure 3. A) Normalized absorption and B) transmission spectra of the slabs functionalized with the different luminophores (yellow and red lines) and of the blue filter (blue lines). The wavelength range considered in the AVT computation corresponds to the white area.

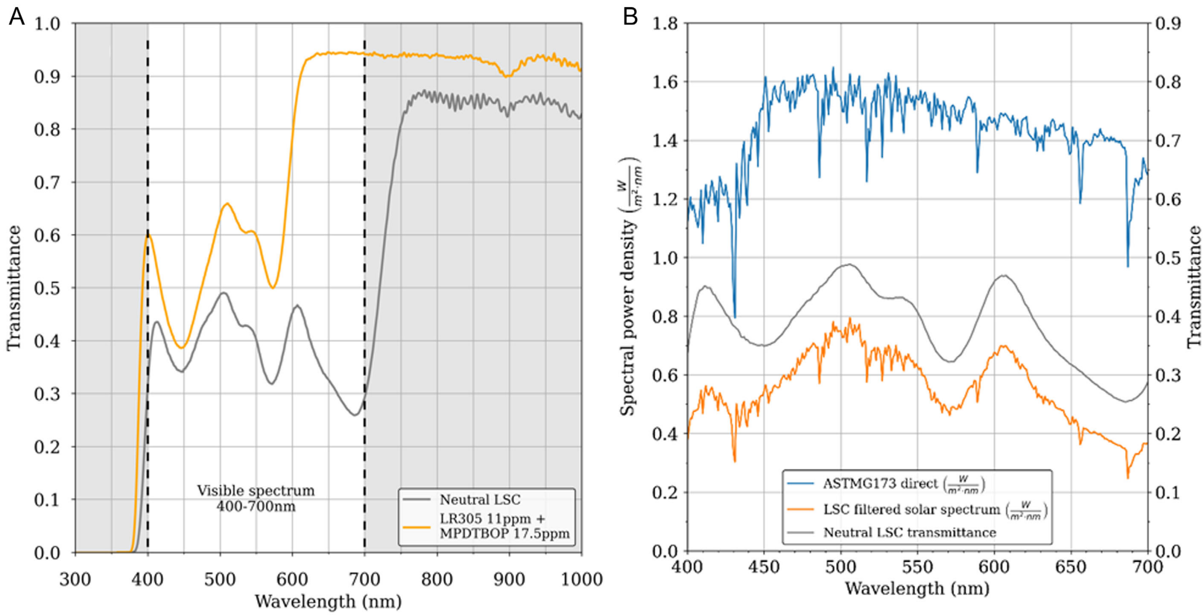

Figure 4. A) Normalized transmission spectra of the window with (gray line) and without (orange line) the blue filter. B) Spectral power density of the direct solar spectrum AM1.5G (blue line), of the same spectrum filtered by the neutral LSC (orange line), as well as its transmission spectrum (gray line). The wavelength range considered in the AVT computation corresponds to the white area.

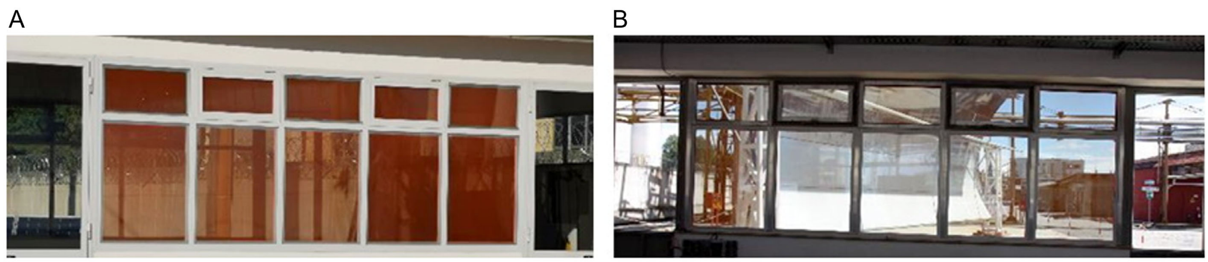

Figure 5. Pictures of the prototypes installed in the Eni Renewable Energy, Magnetic Fusion and Material Science Research Centre in Novara (Italy) viewed from the A) outside and the B) inside of the building. The Prototype 3 used for the indoor characterizations of Figure 7 corresponds the central module, whereas Sample 5 on which the in-depth analysis were performed (see Figure 8A and Table 2) is the rightmost and the leftmost device in Figure 5A,B, respectively.

and MPDTBOP spectra reported in Figure 3 leads to the hypothesis of that this device will present higher self-absorption with respect to an LSC functionalized with a single luminophores. However, utilizing a single luminophore would have necessitated additional customization of the thin film. This customization would be aimed at aligning its absorption spectrum to effectively filter out the spectral components not absorbed by the dye while maintaining a similar relative weight in the transmitted components (see Figure 4B) in order to guarantee a comparable colorimetric balance.

3.2. Colorimetric Analysis

This analysis allows the estimation of the prototype chromatic rendering that was computed thanks to Equation (4) giving a CRI of 93.0, overcoming both the typical values of commercial tungsten-halogen lamps, which range between 85 and 90,[53–55] and the benchmark to be considered an ideal illuminant, 90, thus avoiding unpleasant effects and poor human visual comfort. Moreover, the value obtained for the TCS09 and TCS12 parameters can be considered very good. Presenting a primary reflectance peak around 460 nm and 0 reflectance past 580 nm, TCS12 is a fundamental sample for light sources to have an accurate rendition in the 430–500 nm range. Having a high score of TCS12 can be very challenging for LED sources that use blue light as their primary excitation source, as the emission range in the blue region has a very narrow width (typically 10–15 nm) that fails to cover the entirety of the TCS12 reflectance bandwidth.

TCS09 instead represents how accurately a light source will reproduce saturated red colors, aspect that is traditionally difficult to render for fluorescent lights. TCS09 spectrum is almost entirely composed of red light (wavelength longer than 600 nm); therefore, a low value of TSC09 will alter the color rendering of red hues. The presented prototypes scored a TCS09 value of 92.8, especially considering that most lighting products available on the market rarely specify this value, and when they do, they

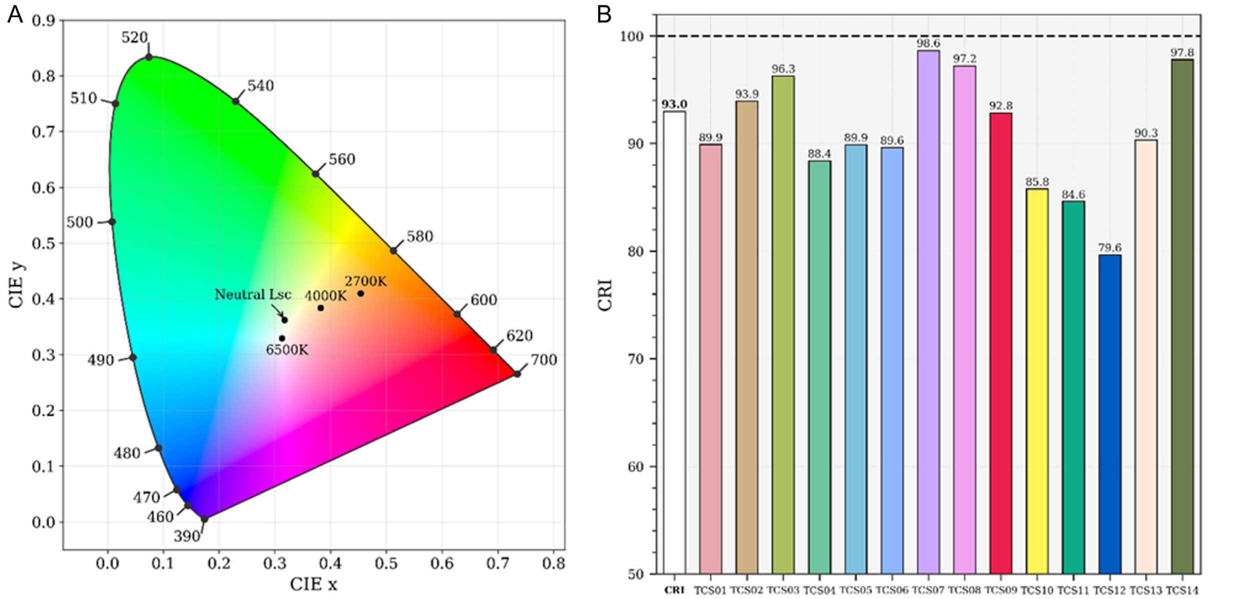

Figure 6. A) CIE 1931 Chromaticity Diagram comparing the properties of the neutral LSC with different light sources. B) CRI plot of the neutral LSC.

hardly guarantee a value higher than 50.[54,55] The plots concerning the colorimetric characterization of the prototypes are shown in **Figure 6**. In Figure 6A, the positions of the light generated by the neutral LSC are compared with the "white light" generated from different sources.[59–61]

3.3. Indoor Electrical Characterization

Figure 7A displays the IV curves of Prototype 3 at different irradiance levels, and Figure 7B shows the increase of the power produced by the module as a function of the increasing irradiance. **Table 1** presents the indoor electrical characteristics of the five prototypes highlighting their PCE computing by using (Equation (6)). The results highlighted on one hand, the increment of the maximum power produced, P_{MAX}, and on the other hand the decrement of the PCE, with respect to the impinging irradiance. Indeed, due to the higher current produced by the cells, P_{MAX} linearly growth with the external irradiation, ranging between 0.59 W and 2.28 W (see Figure 7B), whereas the PCE drops from 0.48% to 0.37%.

These results seem to be unexpected, as the efficiency of silicon solar cells generally decreases proportionally with the

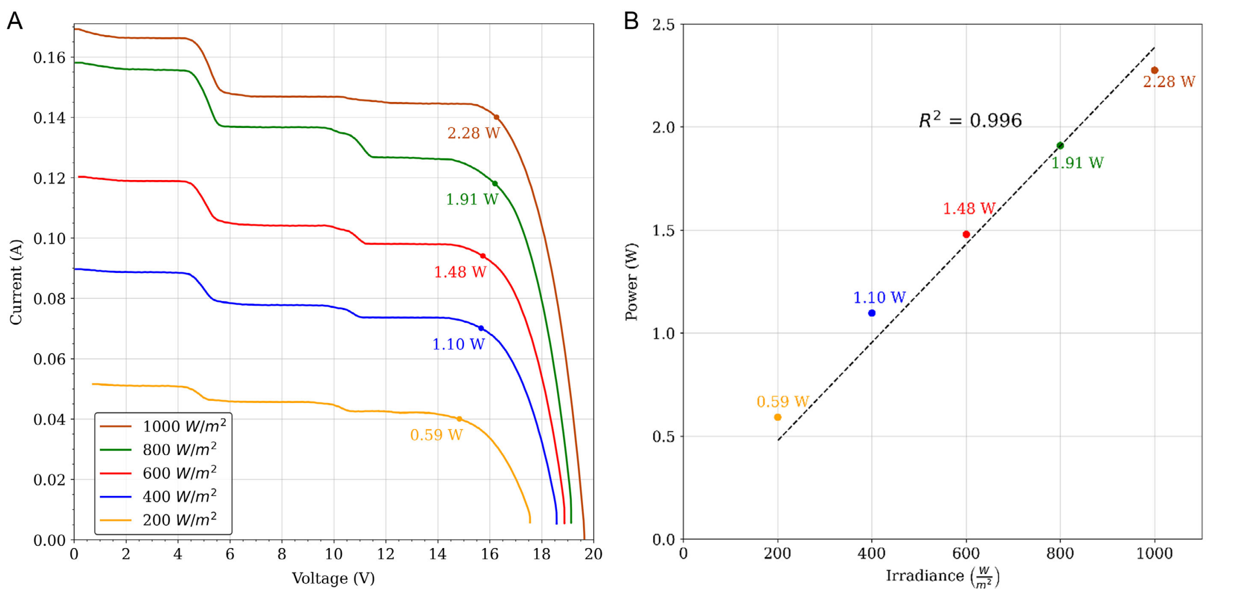

Figure 7. A) IV characteristic curve measured of Prototype 3 when exposed to different irradiance levels highlighting the MPP of each curve. B) MPPs of the module against the different irradiance intensities.

Table 1. Summary of the LSC electrical parameters measured during indoor characterizations, as a function of the impinging irradiance.

E [W m^{-2}]	V_{oc} [V]	I_{sc} [A]	V_{MPP} [V]	I_{MPP} [A]	P_{MAX} [W]	FF	PCE [%]
200	17.82	0.06	14.21	0.04	0.59	0.54	0.48
400	18.71	0.09	15.60	0.07	1.10	0.64	0.45
600	18.98	0.12	16.01	0.09	1.49	0.63	0.41
800	19.21	0.16	15.98	0.12	1.91	0.62	0.39
1000	19.59	0.17	16.26	0.14	2.28	0.67	0.37

irradiance; however, a similar behavior for LSC devices has already been reported by several authors. In particular, Michael G. Debije and Vikram A. Rajkumar[62] highlighted this effect for LSC devices functionalized with Lumogen F 305 dye (BASF) and H. Zhao et al.[63] for LSC device integrating carbon QDs. In particular, the latter stated that the more the light intensity decreases, the more the PCE increases. This is ascribed to a decrease of the absorption efficiency of the QDs at high light intensity. Similarly, for the device presented in this work, the low concentration of organic dyes can explain the lower light absorption capacity of the active slab at high irradiance levels.

All the presented IV curves show secondary knees due to a mismatch in the current produced by the different PV arrays connected in series,[64] effect that may be ascribable to several factors. A possible source is the assembly process, since, although the used configuration is the one providing the best trade-off between the uniformity of the illumination profile reaching the cells and the power produced by the module,[17] it can still generate a small current mismatch.

However, the assembly configuration in which the slab long side is coupled with the PV arrays, and shorter edges are covered with the reflective film ensures the uniformity of the illumination profile exiting from the slab.[17] The current mismatch generated by the assembling process therefore too limited to justify the secondary knees displayed in Figure 7A. The causes of current mismatch must therefore be sought in external irradiance reaching the PV cells with a not uniform profile via different paths with respect to the fluorescent waveguide. The analysis of the possible reasons generating this effect, as well as their contribution in overall phenomenon, is better detailed in the following Section 3.4 Outdoor electrical characterization.

3.4. Outdoor Electrical Characterization

In **Figure 8**A, an in-depth analysis on the electrical performance of one prototype is presented, whereas in Figure 8B, the IV curves related to the five prototypes with their MPPs are reported. The electrical characterizations of Figure 8A were carried out both at the installation site and at the end of the assembly process. The former was done to evaluate the module performance in a real operating environment, whereas the latter to verify the maximum power that could be obtained in a replicable condition. During the second characterization a single LSC panel was coupled with a white diffusive background (WB) showing a power production of 2.81 W, which once installed in the test building decreases to 1.23 W (see **Table 2**). The increase in power production with the WB can be ascribed to the conversion of a portion of the transmitted light thanks to the back diffusion done by the WB.

Comparing the short-circuit current of the prototype, I_{SC}, with that of the PV arrays directly exposed to the sunlight, presented in Table S1, Supporting Information, it is possible to estimate the optical efficiency (OE) of the LSC panels.[58] Considering the onsite measurements for Prototype 5 the OE resulted equal to 1.2, and the presence of the diffusive background doubled the I_{SC} generated by the prototype (see Table 2).

The results presented in Table 2 highlight how the exposition to a uniform illumination (diffusive background) leads to a PCE similar to the one obtained throughout the electrical assessments conducted indoors. The plots displayed in Figure 8A confirm that if subjected to ideal illumination conditions the secondary knee

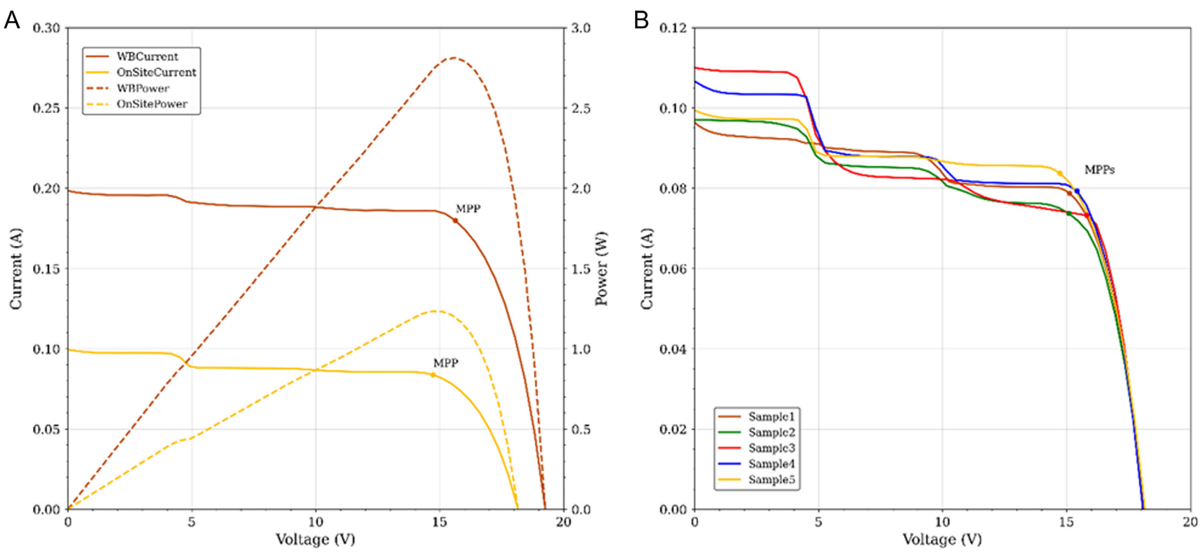

Figure 8. Characteristic IV (continuous lines) and P–V (dashed lines) curves of the whole window (Sample 5, rightmost sample in Figure 5A and leftmost one in Figure 5B). B) On site IV curves of the prototypes with the MPPs.

Table 2. Summary of the performance of one neutral window (prototype 5) tested both on site and with a diffusive background.

	V_{OC} [V]	I_{SC} [A]	V_{MPP} [V]	I_{MPP} [A]	P_{max} [W]	E [W m^{-2}]	FF	PCE [%]
Diffusive background	19.25	0.20	15.63	0.18	2.81	990	0.74	0.47
Onsite	18.16	0.10	14.73	0.08	1.23	880	0.68	0.23

in the IV curve is considerably reduced even if not negligible regardless of whether the electrical performance was measured on site (yellow curve).

Indoor electrical characterization the magnitude of the current mismatch due to the assembly process is too small to justify the secondary knees presented in the reported IV, and it must be combined with other factors having a dominant contribution. Figure 7A and 8A underline that this drop is more evident for high level of irradiance and for measurements performed onsite.

The presence of multiple knees is even more evident in Figure 8B that compares the electrical performance of the five windows measured onsite. Once installed, these prototypes were closed to a large metallic structure lying at a distance varying between 2 and 8 m from the façade hosting the LSC panels. Thus, considering the nonuniform background from the indoor side and the particularly uneven foreground (see Figure 5), the most likely source of the irregular illumination of the PV arrays is the stray light transmitted through the semi-transparent silicone sealant and reflected by the mirror film. In **Figure 9**, a graphical representation useful to better illustrate how the stray light reaches the solar cells is presented.

This hypothesis is confirmed by the characterization reported in Figure S1, Supporting Information, concerning the electrical behavior of the bare arrays mounted on Sample 5, which show a mismatch between the produced current an order of magnitude lower with respect to the one depicted in Figure 8A (≃0.1 mA). However, these can be considered typical working conditions for BIPV devices installed in residential or commercial buildings, as in urban areas the scattering caused by cars, surrounding

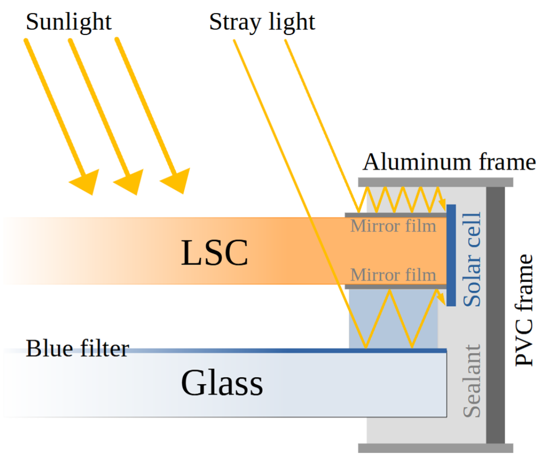

Figure 9. Graphical representation of a cross section of the window frame showing the possible paths of stray light that reaches the solar cells through the semi-transparent silicone sealant because of the reflection on the mirror film.

Table 3. Summary of the electrical performance of the five prototypes installed at Eni "renewable, new energy and material science research centre" Novara (Italy).

Sample	V_{OC} [V]	I_{SC} [A]	V_{MPP} [V]	I_{MPP} [A]	P_{max} [W]	E [W m^{-2}]	FF	PCE [%]
1	18.12	0.10	15.12	0.08	1.19	800	0.68	0.25
2	18.13	0.10	15.09	0.07	1.11	835	0.63	0.22
3	18.09	0.11	15.82	0.07	1.16	850	0.58	0.23
4	18.07	0.11	15.42	0.08	1.22	865	0.63	0.23
5	18.15	0.10	14.73	0.08	1.23	880	0.68	0.23

buildings, or even the diffused light emitted by streetlights, highly affect the uniformity of the radiation impinging on them.

Moreover, it is important to point out that the additional stray light that reach the cells does not negatively affect the power output of the system because, compared with a situation with no stray light, the current of the cells is always increased albeit nonuniformly.

The results concerning the five prototypes PV performance measured after the installation are summarized in **Table 3**. The obtained PV efficiencies are comparable with the ones of large-area LSC panels presented in literature[45,65,66] for both indoor and outdoor characterizations, even considering the additional optical losses due to the colorimetric balance. The real added value of this device lies in its neutral color as this feature allows its integration also in commercial or residential buildings, where neither traditional colored LSCs nor standard PV panels can provide the required high transparency and balanced transmission spectrum. Despite the limited power produced by each window, this is sufficient to run small appliances like air recycling fans, automatic blinds, or LEDs lighting.[66,67]

The autonomous operation of this kind of devices not only increases the building indoor comfort, but they considerably decrease the building energy demand.[14] Moreover, the optical characterizations suggest that the obtained onsite PCE (≃0.23%) could be incremented up to ≃0.5%[46] by preserving the same single-slab structure but acting on the approach used to achieve the indoor neutral color.

4. Conclusions

This research demostrates that optically neutral LSC panels can be obtained from the coupling between a slab functionalized with a bland of colored organic dyes and optical filters.

In particular, the combination of 11 ppm of LR305 and 17.5 ppm of MPDTBOP with the addition of a blue filter leads to the realization of windows having an AVT equal to 38.5%, which is considerably higher with respect to the one of commonly available semi-transparent PV devices. The CRI of 93.0 indicates that the light spectrum emerging from the prototypes is better balanced with respect to the majority of artificial illuminant, thus ensuring an excellent visual comfort for the occupants. Furthermore, the windows' exterior side preserves its characteristic color, thus making this type of photovoltaic window appealing for architectonic contexts in which the building external design requires the application of colored transparent surfaces.

The PCE resulting from the electrical characterizations ranged between 0.23% and 0.47%, highlighting that despite the efficiency limitation due to possible optical losses, the chosen design ensures efficiency values comparable with the ones of large area LSCs reported in literature.

The lare size of these panels increases their attractiveness for BIPV applications, in both commercial and residential buildings. Despite the obtained results, the necessity to improve the overall PCE is evident and the realization of prototypes with a PCE value of 1% can be considered as a reasonable target. This value could be achieved either by increasing the dyes concentration or by pursuing a reduction of the module optical losses. Despite current efficiency limitations, the power generated by the prototypes presented in this work is sufficient to operate stand-alone independent appliances and smart systems, such as a motorized shading system or small ventilation systems. In the building sector, which continually seeks new solutions to enhance energy efficiency, there is ample potential for devices of this kind, as they have the capability to transform specific passive components like windows, covers, and parapet walls into energy sources. The integration of the five prototypes in the Eni "Renewable, New Energies and Material Science Research Centre" will allow in-depth studies on the long-term operational stability of large-area LSCs devices functionalized with this blend of organic dyes and exposed to outdoor environmental conditions. There tests are still ongoing and will be described in a further paper.

Supporting Information

Supporting Information is available from the Wiley Online Library or from the author.

Acknowledgements

This work was carried out in the framework of the research project INSTM1735 OdL 4310346905 funded by Eni and would have been impossible without the support from the Eni "Renewable, New Energies and Material Science Research Centre."

Conflict of Interest

The authors declare no conflict of interest.

Author Contributions

B.P.: Methodology, validation; G.M.: writing—original draft, visualization, writing—review and editing; A.A.: writing—review and editing, data curation; V.D.: visualization, formal analysis; R.M.: methodology, validation, writing; F.M.: methodology, validation, writing; S.Z.: methodology, validation, writing; D.V.: funding acquisition, supervision.

Data Availability Statement

The data that support the findings of this study are available from the corresponding author upon reasonable request.

Keywords

color rendering index, luminescent solar concentrators, neutral colors, photovoltaic windows, semi-transparent solar modules

Received: March 6, 2024
Revised: April 15, 2024
Published online: May 6, 2024

[1] M. Howley, M. Holland, Energy in Ireland 1990–2015 **2016**, http://www.seai.ie/resources/publications/Energy-in-Ireland-1990-2015.pdf (accessed: December 2023).
[2] H. M. Maghrabie, M. A. Abdelkareem, A. H. Al-Alami, M. Ramadan, E. Mushtaha, T. Wilberforce, A. G. Olabi, *Buildings* **2021**, *11*, 11090383.
[3] R. Leonhardt, B. Noble, G. Poelzer, P. Fitzpatrick, K. Belcher, G. Holdmann, *Energy Res. Soc. Sci.* **2022**, *83*, 102350.
[4] S. Fugattini, U. Gulzar, A. Andreoli, L. Carbone, M. Boschetti, P. Bernardoni, M. Gjestila, G. Mangherini, R. Camattari, T. Li, S. Monaco, M. Ricci, S. Liang, D. Giubertoni, G. Pepponi, P. Bellutti, M. Ferroni, L. Ortolani, V. Morandi, D. Vincenzi, R. P. Zaccaria, *Electrochim. Acta* **2022**, *411*, 139832.
[5] B. Mukhopadhyay, D. Das, *Renew. Sustain. Energy Rev.* **2020**, *124*, 109777.
[6] V. Diolaiti, A. Andreoli, P. Bernardoni, G. Mangherini, M. A. Ouelhazi, E. Venczia, M. Ricci, R. Z. Proietti, D. Vincenzi, in *2022 IEEE 22nd Int. Conf. on Nanotechnology (NANO)*, IEEE, New York, NY **2022**, pp. 56–59, https://doi.org/10.1109/nano54668.2022.9928666.
[7] A. Fahrenbruch, R. Bube, *Fundamentals of Solar Cells: Photovoltaic Solar Energy Conversion*, Elsevier, Amsterdam **2012**.
[8] M. Hosenuzzaman, N. A. Rahim, J. Selvaraj, M. Hasanuzzaman, A. B. M. A. Malek, A. Nahar, *Renew. Sustain. Energy Rev.* **2015**, *41*, 284.
[9] M. Boschetti, D. Vincenzi, G. Mangherini, P. Bernardoni, A. Andreoli, M. Gjestila, R. Camattari, S. Fugattini, S. Caramori, V. Cristino, L. Pasti, T. Chenet, C. A. Bignozzi, *Sol. Energy.* **2021**, *228*, 120.
[10] Y. Da, Y. Xuan, Q. Li, *Energy* **2016**, *95*, 200.
[11] S. Sadhishkumar, T. Balusamy, *Renew. Sustain. Energy Rev.* **2014**, *37*, 191.
[12] D. E. Smith, M. D. Hughes, B. Patel, D. A. Borca-Tasciuc, *Energies* **2021**, *14*, 14020455.
[13] E. Biyik, M. Araz, A. Hepbasli, M. Shahrestani, R. Yao, L. Shao, E. Essah, A. C. Oliveira, T. del Caño, E. Rico, J. L. Lechón, L. Andrade, A. Mendes, Y. B. Atlı, *Eng. Sci. Technol.* **2017**, *20*, 833.
[14] A. Ghosh, *Sol. Energy* **2022**, *237*, 213.
[15] I. Zanetti, P. Bonomo, F. Frontini, E. Saretta, Building Integrated Photovoltaics: Product Overview for Solar Building Skins **2017**.
[16] G. Mangherini, V. Diolaiti, P. Bernardoni, A. Andreoli, D. Vincenzi, *Energies* **2023**, *16*, 6901.
[17] P. Bernardoni, G. Mangherini, M. Gjestila, A. Andreoli, D. Vincenzi, *Energies* **2021**, *14*, 14040816.
[18] G. Maggioni, A. Campagnaro, S. Carturan, A. Quaranta, *Sol. Energy Mater. Sol. Cells* **2013**, *108*, 27.
[19] S. F. H. Correia, V. De Zea Bermudez, S. J. L. Ribeiro, P. S. André, R. A. S. Ferreira, L. D. Carlos, *J. Mater. Chem. A* **2014**, *2*, 5580.
[20] J. Bomm, A. Büchtemann, A. J. Chatten, R. Bose, D. J. Farrell, N. L. A. Chan, Y. Xiao, L. H. Slooff, T. Meyer, A. Meyer,

W.G.J.H.M. Van Sark, R. Koole, *Sol. Energy Mater. Sol. Cells* **2011**, *95*, 2087.
[21] M. R. Bergren, N. S. Makarov, K. Ramasamy, A. Jackson, R. Guglielmetti, H. McDaniel, *ACS Energy Lett.* **2018**, *3*, 520.
[22] C. J. Traverse, R. Pandey, M. C. Barr, R. R. Lunt, *Nat. Energy* **2017**, *2*, 849.
[23] B. C. Rowan, L. R. Wilson, B. S. Richards, *IEEE J. Sel. Top. Quantum Electron.* **2008**, *14*, 1312.
[24] Z. Krumer, W.G.J.H.M. van Sark, R. E. I. Schropp, C. de Mello Donegá, *Sol. Energy Mater. Sol. Cells* **2017**, *167*, 133.
[25] M. G. Debije, P. P. C. Verbunt, *Adv. Energy Mater.* **2012**, *2*, 12.
[26] F. Meinardi, F. Bruni, S. Brovelli, *Nat. Rev. Mater.* **2017**, *2*, 9.
[27] R. Zarcone, M. Brocato, P. Bernardoni, D. Vincenzi, *Energy Procedia* **2016**, *91*, 887.
[28] J. Choi, K. Kim, S. J. Kim, *Quantum Dot Assisted Luminescent Hexarhenium Cluster Dye For A Transparent Luminescent Solar Concentrator*, Nature Publishing Group, London, UK **2021**.
[29] Y. Gu, X. Yao, H. Geng, G. Guan, M. Hu, M. Han, *ACS Appl. Mater. Interfaces* **2021**, *13*, 40798.
[30] R. Mazzaro, A. Gradone, S. Angeloni, G. Morselli, P. G. Cozzi, F. Romano, A. Vomiero, P. Ceroni, *ACS Photonics* **2019**, *6*, 2303.
[31] C. Yang, R. R. Lunt, *Adv. Opt. Mater.* **2017**, *5*, 10.
[32] I. Coropceanu, M. G. Bawendi, *Nano Lett.* **2014**, *14*, 4097.
[33] C. S. Erickson, L. R. Bradshaw, S. McDowall, J. D. Gilbertson, D. R. Gamelin, D. L. Patrick, *ACS Energy Lett.* **2014**, *104*, 3461.
[34] C. Li, W. Chen, D. Wu, D. Quan, Z. Zhou, J. Hao, J. Qin, Y. Li, Z. He, K. Wang, *Sci. Rep.* **2015**, *5*, 1.
[35] Y. Zhao, R. R. Lunt, *Adv. Energy Mater.* **2013**, *3*, 1143.
[36] D. A. Chengelis, A. M. Yingling, P. D. Badger, C. M. Shade, S. Petoud, *J. Am. Chem. Soc.* **2005**, *127*, 16752.
[37] A. Sanguineti, A. Monguzzi, G. Vaccaro, F. Meinardi, E. Ronchi, M. Moret, U. Cosentino, G. Moro, R. Simonutti, M. Mauri, R. Tubino, L. Beverina, *Phys. Chem. Chem. Phys.* **2012**, *14*, 6452.
[38] R. Rondão, A. R. Frias, S. F. H. Correia, L. Fu, V. De Zea Bermudez, P. S. André, R. A. S. Ferreira, L. D. Carlos, *ACS Appl. Mater. Interfaces* **2017**, *9*, 12540.
[39] W. Li, X. Wang, J. Lin, X. Meng, L. Wang, M. Wang, Q. Jing, Y. Song, A. Vomiero, H. Zhao, *Nano Energy* **2024**, *122*, 109289.
[40] J. Lin, L. Wang, Q. Jing, H. Zhao, *Chem. Eng. J.* **2024**, *481*, 148441.
[41] C. Yang, M. Moemeni, M. Bates, W. Sheng, B. Borhan, R. R. Lunt, *Adv. Opt. Mater.* **2020**, *8*.
[42] M. Rafiee, S. Chandra, H. Ahmed, S. J. McCormack, *Opt. Mater.* **2019**, *91*, 212.
[43] C. Corrado, S. W. Leow, M. Osborn, I. Carbone, K. Hellier, M. Short, G. Alers, S. A. Carter, *J. Renew. Sustain. Energy* **2016**, *8*.
[44] J. Zhang, M. Wang, Y. Zhang, H. He, W. Xie, M. Yang, J. Ding, J. Bao, S. Sun, C. Gao, *Sol. Energy* **2015**, *117*, 260.
[45] Á. Bognár, S. Kusnadi, L. H. Slooff, C. Tzikas, R. C. G. M. Loonen, M. M. de Jong, J. L. M. Hensen, M. G. Debije, *Renew. Energy* **2020**, *151*, 1141.
[46] G. Mangherini, P. Bernardoni, E. Baccega, A. Andreoli, V. Diolaiti, D. Vincenzi, *Sustainability* **2023**, *15*, 9146.
[47] R. Fusco, L. Gila, L. Caccianotti, A. A. Proto, Luminescent Solar Concentrators Of Neutral Coloration, 20210111360A1, **2021**.
[48] G. Schimperna, L. Gila, Luminescent Solar Concentrator, EP3516704, **2019**.
[49] SunPower, Technical Data Sheet: C50 Solar Cell Mono Crystalline Silicon **2010**.
[50] 3M, Technical Data Sheet: DF2000MA Release B **2015**.
[51] T. Mansencal, M. Mauderer, M. Parsons, N. Shaw, K. Wheatley, S. Cooper, S. Hill, *Color-Sci.* **2020**.
[52] R. R. Lunt, *Appl. Phys. Lett.* **2012**, *101*, 043902.
[53] G. Eder, G. Peharz, R. Trattnig, P. Bonomo, E. Saretta, F. Frontini, C. S. Polo Lopez, H. Rose Wilson, J. Eisenlohr, N. Martín Chivelet, S. Karlsson, N. Jakica, A. Zanelli, Coloured BIPV Market, Research and Development IEA PVPS Task 15, Report IEA-PVPS T15-07: 2019 **2019**, http://iea-pvps.org/index.php?id=task15 (accessed: January 2024).
[54] P. P. Dai, C. Li, X. T. Zhang, J. Xu, X. Chen, X. L. Wang, Y. Jia, X. Wang, Y. C. Liu, *Light Sci. Appl.* **2016**, *5*, 9.
[55] Y. Ohno, *Fourth Int. Conf. Solid State Light* **2004**, *5530*, 88.
[56] W. Naim, V. Novelli, I. Nikolinakos, N. Barbero, I. Dzeba, F. Grifoni, Y. Ren, T. Alnasser, A. Velardo, R. Borrelli, S. Haacke, S. M. Zakeeruddin, M. Graetzel, C. Barolo, F. Sauvage, *JACS Au.* **2021**, *1*, 409.
[57] R. R. Lunt, *Appl. Phys. Lett.* **2012**, *101*, 4738896.
[58] R. H. Inman, G. V. Shcherbatyuk, D. Medvedko, A. Gopinathan, S. Ghosh, *Opt. Express* **2011**, *19*, 24308.
[59] Q. Wang, H. Xu, F. Zhang, Z. Wang, *Optik* **2017**, *129*, 21.
[60] I. Speier, M. Salsbury, *Sixth Int. Conf. Solid State Light* **2006**, *6337*, 63371F.
[61] C. H. Sharp, *J. Opt. Soc. Am.* **1930**, *20*, 62.
[62] M. G. Debije, V. A. Rajkumar, *Sol. Energy* **2015**, *122*, 334.
[63] H. Zhao, G. Liu, S. You, F. V. A. Camargo, M. Zavelani-Rossi, X. Wang, C. Sun, B. Liu, Y. Zhang, G. Han, A. Vomiero, X. Gong, *Energy Environ. Sci.* **2021**, *14*, 396.
[64] D. Roche, H. Outhred, J. R. Kaye, *Prog. Photovoltaics Res. Appl.* **1995**, *3*, 115.
[65] N. Aste, M. Buzzetti, C. Del Pero, R. Fusco, D. Testa, F. Leonforte, *Energy Procedia* **2017**, *105*, 967.
[66] N. Aste, M. Buzzetti, C. Del Pero, R. Fusco, F. Leonforte, D. Testa, *J. Clean. Prod.* **2019**, *219*, 35.
[67] V. Muteri, F. Guarino, S. Longo, L. Bua, M. Cellura, D. Testa, M. Bonzi, *Sustainability* **2022**, *14*, 31.

